

A HIGHLY INCLINED ORBIT FOR THE 110-DAY PERIOD M-DWARF COMPANION KOI-368.01

GEORGE ZHOU^{1,2} AND CHELSEA X. HUANG²

Draft version November 1, 2018

ABSTRACT

We report the detection of asymmetry in the transit light curves of the 110-day period companion to KOI-368, a rapidly rotating A-dwarf. The significant distortion in the transit light curve is attributed to spin-orbit misalignment between the transiting companion and the gravity darkened host star. Our analysis was based on 11 Long Cadence and 2 Short Cadence transits of KOI-368.01 from the *Kepler* mission, as well as stellar parameters determined from our follow-up spectroscopic observation. We measured the true obliquity between the orbit normal and the stellar rotation axis to be 69_{-10}^{+9} °. We also find a secondary eclipse event with depth 29 ± 3 ppm at phase 0.59, from which the temperature of the companion is constrained to 3060 ± 50 K, indicating that KOI-368.01 is a late M-dwarf. The eccentricity is also calculated from the eclipse to be 0.1429 ± 0.0007 . The long period, high obliquity, and low eccentricity of KOI-368.01 allow us to limit a number of proposed theories for the misalignment of binary systems.

Subject headings: binaries: eclipsing—stars: low-mass—techniques: photometric—stars: individual (KOI-368)

1. INTRODUCTION

Spin-orbit alignment is predicted for binary systems by many prominent star formation theories. Binaries formed in clouds with the same net rotation or with disk fragmentation are naturally expected to be in alignment, as confirmed in the majority of systems by indirect measurements from polarisation of circumstellar disks (e.g. Monin et al. 1998; Wheelwright et al. 2011).

Surprisingly, accurate obliquities of close-in stellar binaries are rarely measured. For systems where both the rotation period and spectroscopic rotational line broadening can be measured, the spin-orbit coupling can be estimated (Hale 1994; Harding et al. 2013). Similarly, an approximate obliquity can be estimated by comparing the measured rotational broadening per star against the expected rotation rate of the spectral type (e.g. Weis 1974; Howe & Clarke 2009). From these measurements, we know that spin-orbit alignment is dominant for close-in stellar binaries. Whilst such arguments are statically meaningful, uncertainties for individual systems are large due to the heavy dependence on stellar age and geometry.

Only five equal-mass (Albrecht et al. 2011; Winn et al. 2011; Albrecht et al. 2013) and three unequal-mass binaries (Siverd et al. 2012; Triaud et al. 2013) have obliquities precisely measured using the Rossiter-McLaughlin (RM) effect (Rossiter 1924). Of these measured systems, only the B4-B5 binary δ Herculis (period 10.6 days, eccentricity 0.489) is misaligned. The observational limitations of RM measurements, such as the need for well-timed observations, mean that the sampled binary systems are severely biased towards the short period regime (< 40 days).

On the other hand, the spin-orbit alignment of transiting planets have now been well explored. Some 50

transiting planets have been measured to date, the majority of which also with the RM effect. These observations have revealed the diversity of orbital obliquities for hot-Jupiters (Albrecht et al. 2012), including planets in retrograde and polar orbits (e.g. Bayliss et al. 2010; Addison et al. 2013).

Proposed explanations for the obliquity of stellar binaries are similar to those for planetary systems, including fragmentation of a molecular cloud (Bonnell et al. 1992; Bate et al. 2010), tilting of the protoplanetary disk (Bate et al. 2000), evolution of the stellar spin axis (Rogers et al. 2012), or dynamical interactions (e.g. Wu & Murray 2003; Fabrycky & Tremaine 2007).

In this study, we search for the distorted light curve of transits about rapidly rotating stars due to orbital obliquity. For a gravity darkened rapid rotator (von Zeipel 1924), a companion with non-zero obliquity will successively block different latitudes of the stellar disk that have different levels of gravity darkening, resulting in a distorted and potentially asymmetric light curve (Barnes 2009). This is the only known method that probes both the stellar obliquity and the projected companion orbit obliquity, which gives us a good estimate of the true orbit inclination. The only existing detections of this effect includes the planet sized companion to KOI-13, with a period of 1.8 days (Szabó et al. 2011; Barnes et al. 2011), and δ Her (Philippov & Rafikov 2013).

KOI-368.01 was identified as a Kepler Object of Interest (KOI) in the Batalha et al. (2013) Kepler catalog. The planetary candidate transits an A-type star in an 110 day period orbit. We report the detection of asymmetry in the transit of KOI-368.01, indicative of spin-orbit misalignment for this system. We also report the detection of a secondary eclipse for the system, indicating the companion is of stellar mass.

2. KOI-368 STELLAR PARAMETERS

KOI-368 (KIC 6603043) is an A-dwarf with the revised Kepler Input Catalogue stellar atmosphere param-

¹ Research School of Astronomy and Astrophysics, Australian National University, Cotter Rd, Weston Creek, ACT 2611, Australia; george@mso.anu.edu.au

² Department of Astrophysical Sciences, 4 Ivy Lane, Peyton Hall, Princeton University, Princeton, NJ 08544

eters of $T_{\text{eff}} = 9257 \pm 200$ K, and $\log g = 4.1 \pm 0.3$ (Pinsonneault et al. 2012).

To validate the stellar parameters, we obtained a high resolution spectrum of KOI-368 on 11 September 2012 using the ARC Echelle Spectrograph (ARCES) mounted on the Apache Point Observatory 3.5-meter telescope (APO 3.5m). ARCES is a cross-dispersed optical spectrograph, with slit width of $1.6''$, giving a spectral resolution of $\lambda/\Delta\lambda \approx 31500$ over the wavelength region 3200–10000Å. The spectrum is extracted and reduced using the Echelle package in *IRAF*³.

The fundamental stellar atmosphere parameters (T_{eff} , $\log g$, $[\text{Fe}/\text{H}]$, $v \sin i_{\text{rot}}$) are derived by fitting synthetic spectra to the observed spectrum. A spectral library was generated with the spectral synthesis program SPECTRUM⁴ (Gray & Corbally 1994), using ATLAS9 model atmospheres (Castelli & Kurucz 2004), and the default isotopic line list provided by SPECTRUM, over the wavelength region 4300–6700Å. For each spectral order, we perform a grid search χ^2 minimisation over the ATLAS9 grid, centred about the KIC stellar parameters. We 1) perform an unrestricted grid search to derive a first iteration of stellar parameters, 2) perform the light curve fit (Section §3.4), using the transit to constrain the $\log g$, and 3) re-perform the spectral grid search with $\log g$ fixed. This iterative process is often used in the characterisation of exoplanet host stars, and provides a more constrained $\log g$ than possible using spectral fitting alone (Sozzetti et al. 2007). The final atmosphere parameters are $T_{\text{eff}} = 9200 \pm 200$ K, $\log g = 4.01 \pm 0.01$, $[\text{Fe}/\text{H}] = -0.02 \pm 0.05$, $v \sin i_{\text{rot}} = 79 \pm 4 \text{ km s}^{-1}$, $\rho = 0.221 \pm 0.004 (\text{g cm}^{-3})$, with errors from the scatter between orders. We match these to the Yonsei-Yale isochrones (Yi et al. 2001), via Monte Carlo sampling over the interpolated isochrones, obtaining the values $M_1 = 2.3 \pm 0.1 M_{\odot}$, $R_1 = 2.4 \pm 0.1 R_{\odot}$. The full list of derived stellar properties are given in Table 1. The stellar density is later independently derived from the light curve in Section §3.4, from which we derive a more accurate iteration of stellar parameters.

We measure the host star rotation period by identifying rotational modulation in the Kepler Long Cadence Pre-search Data Conditioning (PDC) light curves (Smith et al. 2012) from Q1-Q9. We masked out the primary transits and performed a Lomb-Scargle periodogram (Lomb 1976) analysis on the light curves. A significant peak at 1.19 days was identified. Assuming the peak is due to rotational modulation, the star rotates with a true velocity of $\sim 100 \text{ km s}^{-1}$, and the rotation axis is inclined to our line of sight by $\sim 50^\circ$ (this is later fitted for in Section §3.4)

3. ORBIT OBLIQUITY FROM LIGHT CURVE ASYMMETRY

3.1. Kepler light curves

We make use of all available public Kepler light curves for our analysis of KOI-368. These include 11 transits (Q0-Q15, more than 1300 day) of Long Cadence (29.4min) data and 2 transits (Q8-Q9) of Short Cadence

(58.84s) data.

To remove the stellar variability, we use the raw flux (SAP_FLUX) obtained from the MAST archive⁵, with the out-of-transit variations corrected by the following steps from Huang et al. (2013):

- a) removal of bad data points;
- b) correction of systematics due to various phenomena of the spacecraft, such as safe modes and tweaks;
- c) a set of cosine functions with minimum period of 1 day;
- d) a 7th order polynomial fit over the out-of-transit regions.

The asymmetry of transit (see Section §3.4) is also reproduced with both the raw light curves and PDC light curves. We use the light curves with above corrections to produce all the fittings below because it gives us the longest flat out-of-transit base line.

3.2. Gravity darkening modelling

The gravity darkening model is generated following Barnes (2009). The temperature profile on the stellar surface is determined by the local effective gravity g_{eff} (von Zeipel 1924). We use the passband gravity darkening coefficient y which directly relates the specific intensity profile of the stellar disk to the effective gravity profile:

$$y = \left(\frac{\partial \ln I(\lambda)}{\partial \ln g_{\text{eff}}} \right)_{T_{\text{eff}}} + \left(\frac{d \ln T_{\text{eff}}}{d \ln g_{\text{eff}}} \right) \left(\frac{\partial \ln I(\lambda)}{\partial \ln T_{\text{eff}}} \right)_{g_{\text{eff}}}. \quad (1)$$

Therefore the ratio of specific intensity $I(\lambda)$ at any position to the intensity at stellar pole $I_{\text{pole}}(\lambda)$ can be written as

$$\frac{I(\lambda)}{I_{\text{pole}}(\lambda)} \propto \left(\frac{g_{\text{eff}}}{g_{\text{pole}}} \right)^y. \quad (2)$$

Note that y relates gravity with intensity, while the commonly used exponent β_{gravity} relates gravity with effective temperature ($y \approx 4\beta_{\text{gravity}}$). The effective gravity is defined as

$$\vec{g}_{\text{eff}} = -\Omega_{\text{grav}}^2 \frac{R_{\text{eq}}^3}{R^2} \hat{r} + \Omega_{\text{rot}}^2 R_{\perp} r_{\perp}. \quad (3)$$

We define Ω_{rot} as the stellar rotation rate and $\Omega_{\text{grav}} = \sqrt{GM/R_{\text{eq}}^3}$ to represent the angular velocity due to gravity at the equator. The definition of the other symbols follow the Eq.10 of Barnes (2009), in which G is the gravitational constant, M is the mass of the star, R and R_{\perp} are the distance from the stellar center and stellar rotation axis to the point of question, respectively. \hat{r} and r_{\perp} are unit vectors indicate the directions of R and R_{\perp} . The effective gravity profile $g_{\text{eff}}/g_{\text{pole}}$ at the stellar surface is then only a function of the oblateness of the star $f = (R_{\text{eq}} - R_{\text{pole}})/R_{\text{eq}}$, the normalised position parameters r , θ , and the dimensionless measure of the rotation rate ($w = \Omega_{\text{rot}}/\Omega_{\text{grav}} = v_{\text{rot}}^2(R/M)$). Since M depends proportionally to R for this spectral type, the uncertainty in the gravity darkening profile depends only weakly on the absolute stellar mass and radius, and primarily on the stellar oblateness f and the rotation velocity v_{rot} . In Figure 1(a), we demonstrate the flux profile computed

³ IRAF is distributed by the National Optical Astronomy Observatory, which is operated by the Association of Universities for Research in Astronomy (AURA) under cooperative agreement with the National Science Foundation.

⁴ <http://www1.apstate.edu/dept/physics/spectrum/spectrum.html> ⁵ http://archive.stsci.edu/kepler/data_search/search.php

for KOI-368. If the companion crosses different latitudes during its transits, the light curves will show asymmetry depending on the misalignment between the companion orbit and stellar rotation axis.

3.3. Secondary eclipse

We search for a secondary eclipse in the *Kepler* long cadence light curve. We find a possible eclipse event at phase 0.59 via a grid search. The depth, inferred eccentricity, and significance of the eclipse is characterised by the global light curve modelling described in Section 3.4. This secondary eclipse event was independently identified by E. Agol and D. Fabrycky, as well as J. Coughlin and the *Kepler* team.

3.4. Fitting of system parameters

The transit light curves are modeled using the Nelson & Davis (1972) model, implemented in an adaptation of the JKTEBOP code (Popper & Etzel 1981; Southworth et al. 2004). The relevant free parameters in the transit model are orbital period P , transit centre T_0 , normalised radius sum $(R_1 + R_2)/a$, radius ratio R_2/R_1 , line of sight inclination i . To allow for a secondary eclipse, we also fit for the surface brightness ratio S_2/S_1 , and eccentricity components $e \cos \omega$ and $e \sin \omega$. The quadratic limb darkening coefficients are fitted for in an initial minimisation routine, then held fixed for subsequent analyses. The final values do not deviate significantly from estimates by Sing (2010). Jump parameters modelling gravity darkening include the sky-projected orbit obliquity angle λ , stellar oblateness factor f , projected stellar obliquity i_{rot} (with initial value taken from Section §2), and the *Kepler* band gravity darkening exponent y , with initial value calculated from Claret & Bloemen (2011). A constant flux baseline offset for each transit is removed before the global fitting. For *Kepler* long cadence data, the model is modified by a 30 minute boxcar smooth. The best fit parameters and the posterior probability distribution is explored via a Markov chain Monte Carlo (MCMC) analysis, using the *emcee* MCMC ensemble sampler (Foreman-Mackey et al. 2012). For each transit, we scale the flux errors such that the reduced χ^2 are at unity. This allows for errors other than photon noise to be taken into account.

Figure 1 plots the phase folded transit and eclipse light curves of KOI-368.01 and the best fit standard and gravity darkened models. The best fit standard model cannot explain the significant in-transit asymmetry observed.

The best fit parameters are presented in Table 1. The posterior probability distributions for relevant parameters are plotted in Figure 2. We did not detect transit timing variations, consistent with previous studies (e.g. Mazeh et al. 2013).

We find a best fit projected obliquity value of $\lambda = 36_{-17}^{+23}^\circ$, and a projected stellar obliquity of $i_{\text{rot}} = 55_{-10}^{+3}^\circ$. The derived true spin-orbit obliquity of KOI-368.01 is $69_{-10}^{+9}^\circ$, indicating that it is orbiting in a highly inclined orbit.

Note that due to the degeneracy between the geometries of λ and $(180^\circ - \lambda)$, we cannot distinguish between prograde and retrograde orbits using this method. We conservatively choose the prograde solution for the quoted angles in this paper.

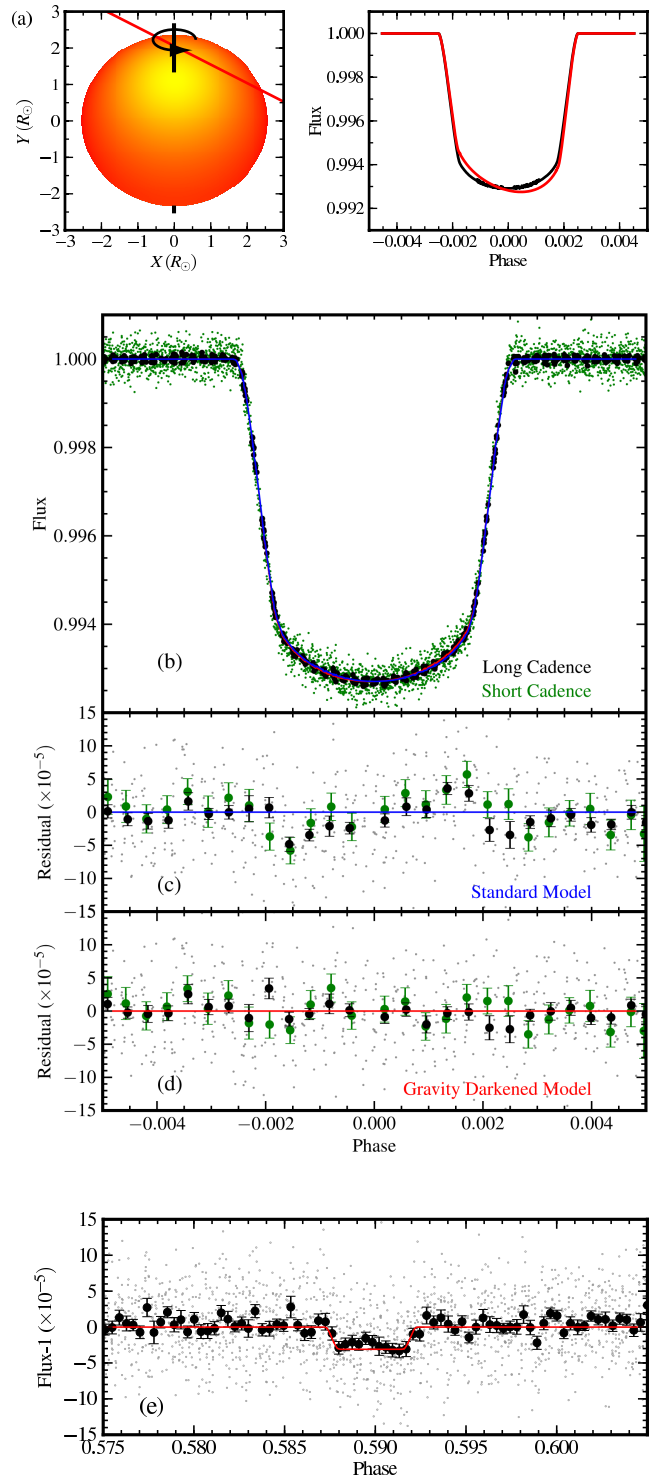


Figure 1. (a) The flux ratio distribution at the surface of KOI-368 is plotted on the left, with $i_{\text{rot}} = 45^\circ$ and exaggerated oblateness parameters of $f = 0.2$, $y = 1.0$. An example transit path with projected obliquity of 30° is marked in red (grey). The corresponding light curve is plotted on the right (in red). This is the best fit configuration for KOI-368.01. For comparison, the best fit light curve without considering gravity darkening is also shown in black. (b) Phase folded transit of KOI-368.01. Long cadence observations are plotted in black, short cadence in green. The best fit standard transit model is plotted in blue, gravity darkened model in red. These two models are visually indistinguishable at this scale, but the difference is statistically significant. (c) Residuals to the standard transit model. The long cadence data are plotted in full as gray dots, and as 1 hour binned intervals in black, short cadence binned residuals in green. (d) Residuals to the gravity darkened transit model. (e) The secondary eclipse event is plotted with the best fit model.

Table 1
KOI-368 System properties

| Parameter | Kepler Catalog | Standard Model | Gravity Darkened Model |
|---------------------------------------------------|-------------------|------------------------|------------------------|
| Photometric magnitudes | | | |
| B^a | 11.30 | - | - |
| V^a | 11.02 | - | - |
| J^b | 11.11 | - | - |
| H^b | 11.09 | - | - |
| K^b | 11.08 | - | - |
| K_p | 11.375 | - | - |
| Spectroscopic parameters | | | |
| T_{eff} (K) | 9257 ± 200 | 9200 ± 200 | - |
| [Fe/H] | -0.3 ^c | -0.02 ± 0.05 | - |
| $v \sin i_{\text{rot}}$ (km s ⁻¹) | - | 79 ± 4 | - |
| Lightcurve fitting parameters ^b | | | |
| Period (Days) | 110.32160 ± 5 | 110.321645^{+6}_{-5} | 110.32164^{+1}_{-1} |
| T_0 (BJD - 2454000) | 1030.3645 ± 2 | 1030.36409^{+3}_{-5} | 1030.36437^{+2}_{-3} |
| $(R_2 + R_1)/a$ | 0.02119 ± 6 | 0.02097^{+5}_{-3} | 0.0206^{+1}_{-1} |
| R_2/R_1 | 0.08453 ± 3 | 0.08408^{+2}_{-5} | 0.0863^{+4}_{-4} |
| i | 89.38 | 89.204^{+5}_{-2} | 89.235^{+9}_{-7} |
| $e \cos \omega$ | - | 0.1417^{+1}_{-1} | 0.1416^{+1}_{-1} |
| $e \sin \omega$ | - | -0.012^{+3}_{-7} | -0.019^{+4}_{-5} |
| S_2/S_1 | - | 0.0045^{+2}_{-2} | 0.0039^{+3}_{-3} |
| f | - | - | 0.052^{+3}_{-3} |
| y | - | - | 0.20^{+6}_{-4} |
| λ | - | - | 36^{+23}_{-17} |
| i_{rot} | - | - | 55^{+3}_{-10} |
| Derived parameters | | | |
| ρ_1 (g cm ⁻³) ^e | - | 0.216 ± 0.003 | 0.221 ± 0.004 |
| M_1 (M_{\odot}) | - | 2.3 ± 0.1 | 2.3 ± 0.1 |
| R_1 (R_{\odot}) | 2.1 ± 0.9 | 2.5 ± 0.1 | 2.4 ± 0.1 |
| $\log g$ | 4.1 ± 0.3 | 4.02 ± 0.01 | 4.02 ± 0.01 |
| Age (Gyr) | 0.51 ± 0.09 | 0.49 ± 0.06 | 0.48 ± 0.06 |
| Luminosity (L_{\odot}) | - | 38 ± 5 | 38 ± 6 |
| Distance (kpc) | - | 1.07 ± 0.05 | 1.07 ± 0.05 |
| R_2 (R_{\odot}) | 0.18 ± 0.08 | 0.209 ± 0.007 | 0.211 ± 0.006 |
| True Obliquity (°) | - | - | 69^{+9}_{-10} |
| e | - | 0.142 ± 0.001 | 0.1429 ± 0.0007 |
| $T_{2,\text{eff}}$ | - | 3080 ± 50 | 3060 ± 50 |

^a Tycho catalogue

^b 2MASS catalogue

^c Assumed

^d Uncertainties quoted are for the last significant figure

^e Derived from light curve fit

Using the phase and duration of the secondary eclipse, we obtain an eccentricity of $e = 0.1429 \pm 0.0007$. The expected transit duration for a circular orbit transit is 12.5 hours. The ratio between the observed and circular expected transit durations give an eccentricity estimate of $e = 0.07^{+0.18}_{-0.07}$, with degeneracies constrained by the lack of ingress-egress duration variations. This is consistent with the eccentricity derived from the secondary eclipse phase.

The light curve asymmetry can not be reproduced by the in-transit velocity change of an eccentric orbit (Barnes 2007) or by the photometric RM effect (Shporer et al. 2012; Groot 2012), both of which result in light curve distortions at least an order of magnitude smaller than that observed.

We also fit a gravity darkening exponent for KOI-368 of $y = 0.20^{+0.06}_{-0.04}$ ($\beta_{\text{gravity}} \approx 0.05$). This is significantly

lower than simple theoretical model predictions, which is also seen for DI Her (Philippov & Rafikov 2013).

4. NATURE OF THE KOI-368 SYSTEM

4.1. Excluding blend scenarios

To constrain the possible blend scenarios for KOI-368, we obtained an image of the object using the APO 3.5m Echelle Slitviewer camera. The camera has a field of view of $63.6''$ and pixel scale of $0.133'' \text{pixel}^{-1}$. The full width half maximum of the point spread function is $1''$. The closest companion brighter than 20 mag is more than $20''$ away from KOI-368 (See Figure 3(a)). We can exclude blend sources with separations greater than $\sim 1''$ from the object.

We can also constrain the possibility of blends by searching for centroid displacements in and out of transit. The displacements are given by the flux weighted

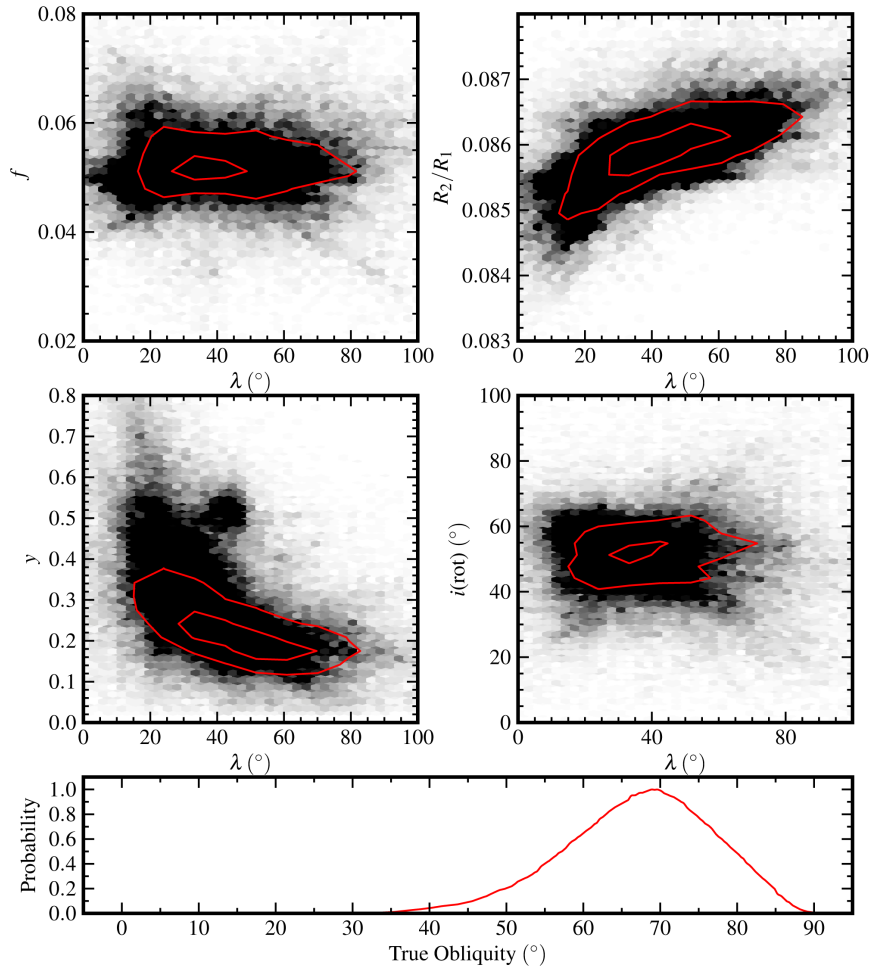


Figure 2. Posterior probability distributions showing the correlation between the projected obliquity λ and stellar oblateness f , radius ratio R_2/R_1 , gravity darkening exponent y , projected stellar obliquity i_{rot} . The contours mark the 1 and 2σ confidence regions. The posterior probability distribution for the true obliquity is plotted on the bottom panel.

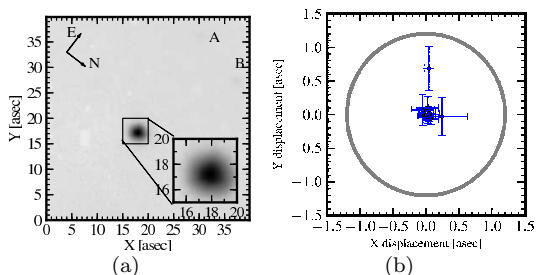


Figure 3. Left: Image of KOI-368 from APO 3.5m Echelle Slitviewer camera, within $40 \times 40''$ area. The two companions brighter than 20 magnitude (marked out as A and B), are $\sim 20''$ away. Insert shows the target PSF. The half width radius of the PSF is $1''$. The shape of PSF is not visibly elongated. Right: Centroid analysis of KOI-368. The transit depth normalised centroids displacement between in-transit and out-transit for all 11 transits are shown. This indicates that the transit signal must be from source $> 1''$ (the black circle).

first momentum centroids produced by Kepler pipeline. We correct for the low frequency (> 5 day) trends in the centroids with a 7th order polynomial around each transit. The displacements between the mean centroids in- and out-of-transit, weighted by the transit depth

(Chaplin et al. 2013), are shown in Figure 3(b). The uncertainties are computed assuming a Gaussian distribution for centroids in each transit. The lack of displacement allows us to rule out an eclipsing neighbour $> 1''$ away.

4.2. KOI-368.01 is an M-dwarf

We can constrain the secondary eclipse to be of depth 29 ± 3 ppm. Using spectral models from (Gustafsson et al. 2008), and integrating over the Kepler band, we find the temperature of the companion to be 3060 ± 60 K. Given that the derived radius of the companion is $0.211 \pm 0.006 R_{\odot}$, the companion is most consistent with an M-dwarf.

5. DISCUSSION

We characterised the asymmetric transit and eclipse light curve of KOI-368.01, and found it to be an M-dwarf companion orbiting in a highly inclined (69^{+9}_{-10}), near-circular ($e = 0.1429 \pm 0.0007$) orbit about a rapidly rotating A-dwarf.

KOI-368 is a distinct system in the period-obliquity space, in the context of both binary and planetary systems (Figure 4). With a period of 110.3 days, KOI-368

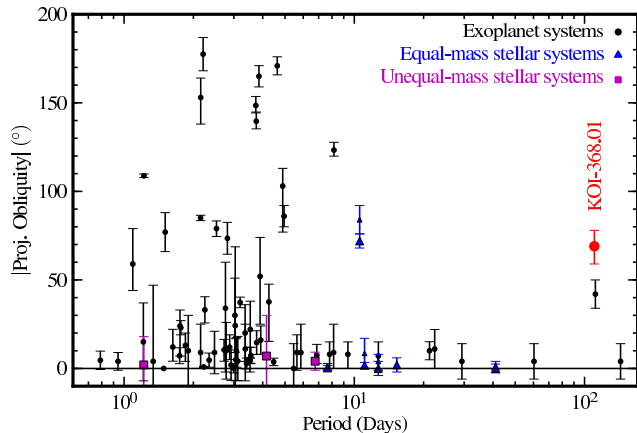


Figure 4. The obliquities of binary systems are plotted against their orbital period. Equal-mass (same spectral type components) stellar systems are marked by blue triangles, with the obliquity of the primary and secondary differentiated by the symbol size (Albrecht et al. 2011; Winn et al. 2011; Harding et al. 2013; Albrecht et al. 2013). Unequal-mass system host stars are labelled by magenta squares (Siverd et al. 2012; Triaud et al. 2013). Exoplanet hosts are plotted in black.

is one of the longest period systems for which spin-orbit alignment has been precisely measured. Other measured highly misaligned systems mostly have shorter period orbits, such as DI Her (10.55 days). Curiously, the orbit of KOI-368.01 is almost identical with the planet HD80606b (111.4 day, $e = 0.93$) in both period and projected orbit obliquity, but with a much lower eccentricity. HD80606b can be explained satisfactorily with Kozai cycle excited by its main-sequence companion 1000 AU away (Wu & Murray 2003; Fabrycky & Tremaine 2007). For KOI-368.01 to be in a high eccentricity migration track, one would expect $e \gtrsim 0.8$, such that the final semi-major axis would be $a < 0.1\text{AU}$. The age of the system is 500 Myrs, whilst the circularisation timescale of this system is much longer than the Hubble time. Alternatively, the high obliquity of this system can be excited by a third body in this system with Kozai mechanism (e.g. Fabrycky & Tremaine 2007; Naoz et al. 2011; Katz et al. 2011) after migrated to the current location. More complex dynamic interactions, such as sequential Kozai migration, can also result in the current configuration (e.g. Narita et al. 2012).

While the obliquity of KOI-368 is also possibly primordial, we can limit the main scenarios for stellar binary misalignment. Simple rotational fragmentation of molecular clouds results in aligned systems. Bonnell et al. (1992) proposed that rotational fragmentation of a highly elongated, tilted, molecular cloud can form misaligned binaries. However, the systems produced by this mechanism tend to have a high initial eccentricity (0.4-0.9). Chaotic accretion has also been suggested as a mechanism for tilting the circumstellar disk (Bate et al. 2010), but results in a misaligned low-mass disk that is unlikely to form stellar mass companions.

We highlight the advantages of this technique in measuring spin-orbit alignments for long-period systems. Ground based RM observations require careful planning, fortunate weather, and are limited in transit duration. Observations of KOI-368 are also limited by its high T_{eff} and large $v \sin i_{\text{rot}}$. Measuring spin-orbit alignment via

star-spot crossings, the only other technique to date to yield results for such long-period systems, is severely biased towards binaries in perfect spin-orbit alignment, and will not identify systems like KOI-368. The high-precision photometry from *Kepler* means that measurements of orbit obliquity from companions about rapidly rotating stars, in conjunction with measurements of the stellar obliquity, are crucial in exploring the dynamics of long-period stellar binaries and planetary systems.

The authors thank the reviewers for their insightful suggestions, G.Á. Bakos for his comments on the letter draft, J.D. Hartman and C. Petrovich for helpful discussions, W.A. Bhatti, J.L. Prieto, and S. Dong for the APO 3.5 m observations. We thank independent comments by E. Agol & D. Fabricky and J. Coughlin & the Kepler team for bringing to our attention the secondary eclipse event; A. Shporer for the photometric RM effect. Work by XCH is supported by the NASA NNX12AH91H and NSF AST1108686 grants. Work by GZ is supported by the NASA NNX12AH91H grant and the Princeton University VSRC program.

REFERENCES

- Addison, B. C., Tinney, C. G., Wright, D. J., et al. 2013, ArXiv e-prints
- Albrecht, S., Setiawan, J., Torres, G., Fabrycky, D. C., & Winn, J. N. 2013, *ApJ*, 767, 32
- Albrecht, S., Winn, J. N., Carter, J. A., Snellen, I. A. G., & de Mooij, E. J. W. 2011, *ApJ*, 726, 68
- Albrecht, S., Winn, J. N., Johnson, J. A., et al. 2012, *ApJ*, 757, 18
- Barnes, J. W. 2007, *PASP*, 119, 986
- . 2009, *ApJ*, 705, 683
- Barnes, J. W., Linscott, E., & Shporer, A. 2011, *ApJS*, 197, 10
- Batalha, N. M., Rowe, J. F., Bryson, S. T., et al. 2013, *ApJS*, 204, 24
- Bate, M. R., Bonnell, I. A., Clarke, C. J., et al. 2000, *MNRAS*, 317, 773
- Bate, M. R., Lodato, G., & Pringle, J. E. 2010, *MNRAS*, 401, 1505
- Bayliss, D. D. R., Winn, J. N., Mardling, R. A., & Sackett, P. D. 2010, *ApJ*, 722, L224
- Bonnell, I., Arcoragi, J.-P., Martel, H., & Bastien, P. 1992, *ApJ*, 400, 579
- Castelli, F., & Kurucz, R. L. 2004, ArXiv Astrophysics e-prints
- Chaplin, W. J., Sanchis-Ojeda, R., Campante, T. L., et al. 2013, *ApJ*, 766, 101
- Claret, A., & Bloemen, S. 2011, *A&A*, 529, A75
- Fabrycky, D., & Tremaine, S. 2007, *ApJ*, 669, 1298
- Foreman-Mackey, D., Hogg, D. W., Lang, D., & Goodman, J. 2012, ArXiv e-prints
- Gray, R. O., & Corbally, C. J. 1994, *AJ*, 107, 742
- Groot, P. J. 2012, *ApJ*, 745, 55
- Gustafsson, B., Edvardsson, B., Eriksson, K., et al. 2008, *A&A*, 486, 951
- Hale, A. 1994, *AJ*, 107, 306
- Harding, L. K., Hallinan, G., Konopacky, Q. M., et al. 2013, *A&A*, 554, A113
- Howe, K. S., & Clarke, C. J. 2009, *MNRAS*, 392, 448
- Huang, X., Bakos, G. Á., & Hartman, J. D. 2013, *MNRAS*, 429, 2001
- Katz, B., Dong, S., & Malhotra, R. 2011, *Physical Review Letters*, 107, 181101
- Lomb, N. R. 1976, *Ap&SS*, 39, 447
- Mazeh, T., Nachmani, G., Holczer, T., et al. 2013, ArXiv e-prints
- Monin, J.-L., Menard, F., & Duchene, G. 1998, *A&A*, 339, 113
- Naoz, S., Farr, W. M., Lithwick, Y., Rasio, F. A., & Teyssandier, J. 2011, *Nature*, 473, 187
- Narita, N., Takahashi, Y. H., Kuzuhara, M., et al. 2012, *PASJ*, 64, L7

- Nelson, B., & Davis, W. D. 1972, *ApJ*, 174, 617
- Philippov, A. A., & Rafikov, R. R. 2013, *ApJ*, 768, 112
- Pinsonneault, M. H., An, D., Molenda-Żakowicz, J., et al. 2012, *ApJS*, 199, 30
- Popper, D. M., & Etzel, P. B. 1981, *AJ*, 86, 102
- Rogers, T. M., Lin, D. N. C., & Lau, H. H. B. 2012, *ApJ*, 758, L6
- Rossiter, R. A. 1924, *ApJ*, 60, 15
- Shporer, A., Brown, T., Mazeh, T., & Zucker, S. 2012, *New Astronomy*, 17, 309
- Sing, D. K. 2010, *A&A*, 510, A21
- Sivard, R. J., Beatty, T. G., Pepper, J., et al. 2012, *ApJ*, 761, 123
- Smith, J. C., Stumpe, M. C., Van Cleve, J. E., et al. 2012, *PASP*, 124, 1000
- Southworth, J., Maxted, P. F. L., & Smalley, B. 2004, *MNRAS*, 351, 1277
- Sozzetti, A., Torres, G., Charbonneau, D., et al. 2007, *ApJ*, 664, 1190
- Szabó, G. M., Szabó, R., Benkő, J. M., et al. 2011, *ApJ*, 736, L4
- Triaud, A. H. M. J., Hebb, L., Anderson, D. R., et al. 2013, *A&A*, 549, A18
- von Zeipel, H. 1924, *MNRAS*, 84, 684
- Weis, E. W. 1974, *ApJ*, 190, 331
- Wheelwright, H. E., Vink, J. S., Oudmaijer, R. D., & Drew, J. E. 2011, *A&A*, 532, A28
- Winn, J. N., Albrecht, S., Johnson, J. A., et al. 2011, *ApJ*, 741, L1
- Wu, Y., & Murray, N. 2003, *ApJ*, 589, 605
- Yi, S., Demarque, P., Kim, Y.-C., et al. 2001, *ApJS*, 136, 417